Journal of Materials Chemistry A

PAPER

View Article Online
View Journal | View Issue

Cite this: *J. Mater. Chem. A*, 2018, **6**, 20813

Exceptional TcO_4^- sorption capacity and highly efficient ReO_4^- luminescence sensing by Zr^{4+} MOFs†

Sofia Rapti,‡[a] Stavros A. Diamantis,‡[b] Argyro Dafnomili,‡[b] Anastasia Pournara,[a] Euaggelia Skliri,[c] Gerasimos S. Armatas,[c] Athanassios C. Tsipis,[a] Ioannis Spanopoulos,[d] Christos D. Malliakas,[d] Mercouri G. Kanatzidis,[d] John C. Plakatouras,*[a] Fotini Noli,*[b] Theodore Lazarides*[b] and Manolis J. Manos*[a]

Received 14th August 2018
Accepted 1st October 2018

DOI: 10.1039/c8ta07901c

rsc.li/materials-a

The sorption properties of $[Zr_6O_4(OH)_4(NH_3^+\text{-BDC})_6]Cl_6\cdot xH_2O$ (**MOR-1**) and $H_{16}[Zr_6O_{16}(H_2PATP)_4]Cl_8\cdot xH_2O$ (**MOR-2**) towards ReO_4^- and TcO_4^- were studied in detail. Both **MOR-1** and **MOR-2** are very effective sorbents for ReO_4^- and TcO_4^- anions, with **MOR-2** showing the highest sorption capacity (up to 4.1 ± 0.4 mmol g^{-1}) among the known metal organic materials. Importantly, the exceptional sorption capacity of **MOR-2** is retained even under conditions simulating acidic nuclear waste. In addition, **MOR-1** and **MOR-2** exhibit selective luminescence ReO_4^- sensing properties, demonstrated for the first time for MOF materials.

Introduction

The treatment of nuclear waste effluents represents a major cause for global concern.[1] Technetium primarily existing in its oxo-anionic form TcO_4^- is considered among the most hazardous radiation-derived contaminants in nuclear waste, since it has a long half-life ($t_{1/2} = 2.13 \times 10^5$ years) and high environmental mobility.[2] A common and successful method of capturing TcO_4^- is ion exchange and several ion exchange materials have been investigated so far including organic resins/polymers and inorganic sorbents.[2–6] Nevertheless, new TcO_4^- sorbents are needed with enhanced properties, such as superior sorption capacities and selectivity, higher sorption rates, reusability *etc.*, aimed at real applications.

Recently, metal organic frameworks (MOFs), decorated with organic groups having a strong binding affinity for toxic ions, have emerged as a new category of promising sorbents.[7,8] MOFs can combine the organic functionalities of amorphous organic resins (strong binding groups) and the ordered porous structure of inorganic materials and may thus be considered as the next generation of sorbent materials. So far, reports on the use of MOFs for removal of TcO_4^- or ReO_4^-, a surrogate of pertechnetate, from water are limited.[9–13]

Additionally, fluorescent MOFs that display selective and rapid sorption of certain species are excellent candidates for sensing applications. The sorbed species (analytes) interact with the MOF's fluorophores bringing about measurable changes in its fluorescence properties which, in turn, may be used for the recognition and/or quantification of the targeted species.[14] An additional property that renders MOFs potentially excellent luminescent sensory materials is their ability to show strongly enhanced detection signals due to the exciton migration within their framework in a manner analogous to that observed in fluorescent conjugated polymers and dendrimers.[15] In such materials an excited state (exciton), initially formed through light absorption by a fluorescent unit, may diffuse along a chain of connected chromophores before encountering a bound analyte.[16] This way a single binding event may affect a large number of fluorophores.

To the best of our knowledge, no MOF has been so far reported as a luminescent sensor for ReO_4^-. The development of fluorimetric methods for the rapid determination of ReO_4^- will be a useful tool in ion exchange studies as perrhenate ion exchange is a model for TcO_4^- sorption investigations. So far, Re(VII) analysis is made primarily *via* costly methods such as ICP-AES and MS, whereas inexpensive colorimetric analytical methods for ReO_4^- determination suffer from relatively low sensitivity and the need for time-consuming sample pre-treatment processes.[17]

Herein, we report the ReO_4^- and TcO_4^- sorption properties of two Zr^{4+} MOFs, namely $[Zr_6O_4(OH)_4(NH_3^+\text{-BDC})_6]Cl_6\cdot xH_2O$

[a]*Department of Chemistry, University of Ioannina, 45110 Ioannina, Greece. E-mail: iplakatu@cc.uoi.gr; emanos@cc.uoi.gr*

[b]*Department of Chemistry, Aristotle University of Thessaloniki, 54124 Thessaloniki, Greece. E-mail: noli@chem.auth.gr; tlazarides@chem.auth.gr*

[c]*Department of Materials Science and Technology, University of Crete, 71003 Heraklion, Greece*

[d]*Department of Chemistry, Northwestern University, Evanston, IL 60208, USA*

† Electronic supplementary information (ESI) available: Experimental and theoretical result details, characterization data, various sorption and luminescence graphs. See DOI: 10.1039/c8ta07901c

‡ These authors contributed equally.

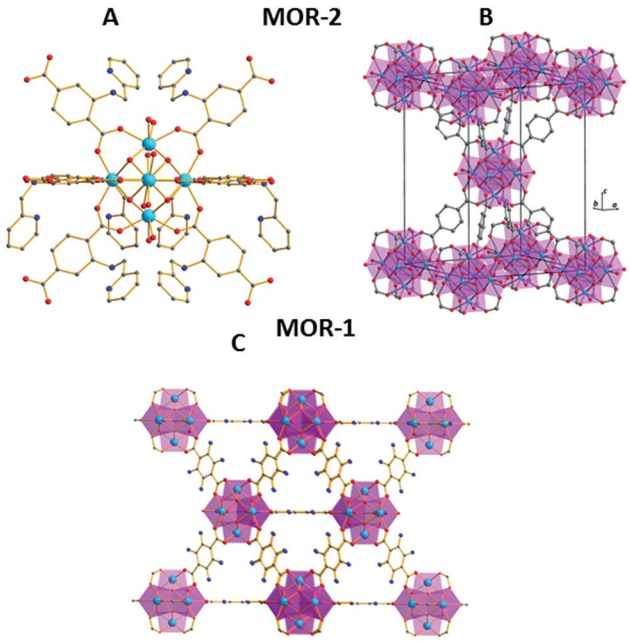

Fig. 1 Representation of the building unit of MOR-2 and its 8-connected framework (A, B)[19] and a part of the 12-connected framework of MOR-1 (ref. 18) (C). Color code: Zr, sky blue; O, red; N, blue; C, grey (H atoms were omitted for clarity).

(**MOR-1**) and $H_{16}[Zr_6O_{16}(H_2PATP)_4]Cl_8 \cdot xH_2O$ (**MOR-2**) (NH_2–H_2BDC = 2-amino-terephthalic acid; H_2PATP = 2-((pyridin-1-ium-2-ylmethyl)ammonio)terephthalate) (Fig. 1), which have been previously tested as sorbents for Cr(VI).[18,19]

MOR-1 and **MOR-2** are highly efficient sorbents for ReO_4^- and TcO_4^-, with **MOR-2** showing the highest ReO_4^- and TcO_4^- sorption capacities (up to 4.1 ± 0.4 mmol g^{-1}) reported among the MOFs and most of other known sorbents. Remarkably, the high sorption capacity of **MOR-2** was retained even under extremely acidic conditions (1 M HNO_3), indicating this material as a promising candidate for remediation of acidic nuclear waste. Furthermore, **MOR-2** in its composite form with alginic acid (HA) was utilized in an ion exchange column, which shows capability for ~100% removal of ReO_4^- from water and can be regenerated and reused for several cycles with almost no loss of its initial sorption capacity. Combined experimental and theoretical data revealed that the enhanced ReO_4^-/TcO_4^- sorption by **MOR-2** is due to the strong interaction of the anionic species with the ammonium/pyridinium functional groups of the MOF as well as the binding of ReO_4^-/TcO_4^- anions into the Zr_6 core. Finally, **MOR-1** and **MOR-2** were found to be exceptional luminescent sensors for ReO_4^- showing high sensitivity (detection limits down to 0.15–0.3 ppm) and selectivity for this species towards various competitive anions. Such luminescence sensing property of MOFs is demonstrated for the first time in this work.

Results and discussion

a. ReO_4^- batch sorption studies

The ReO_4^- sorption properties of **MOR-1** and **MOR-2** were investigated in detail in order to determine the efficiency of these materials for perrhenate capture and consequently, their potential to be used as TcO_4^- sorbents. The capture of ReO_4^- by **MOR-1** and **MOR-2** was found to be remarkably fast, as the sorption equilibrium is reached within 5–6 min for both materials (Fig. S1, ESI†). **MOR-2** appeared more effective than **MOR-1**, since **MOR-2** could remove ~72% of the initial ReO_4^- content (0.58 mM, pH ~ 7) of the solution, whereas **MOR-1** showed ~51% ReO_4^- removal capacity. The higher efficiency of **MOR-2** as ReO_4^- sorbent will become more apparent below in the discussion of the sorption isotherm results. The kinetic data for **MOR-1** and **MOR-2** can be fitted with Lagergren's first order and pseudo-second order[18,19] models, respectively (Fig. S2 and S3†).For comparison, the ReO_4^- sorption kinetics for the $[Zr_6O_4(OH)_4(BDC)_6]$ (UiO-66) MOF (H_2BDC = terephthalic acid)[20] was also investigated (Fig. S1†). The results revealed ~21% ReO_4^- removal capacity for the UiO-66 material, significantly lower than the perrhenate capture by **MOR-1** and **MOR-2**. Presumably, the presence of ammonium/pyridinium functional groups that can strongly interact with ReO_4^- (see below) results in the significantly higher ReO_4^- sorption efficiency of **MOR-1** and **MOR-2** compared to that of the unfunctionalized UiO-66 material. Kinetic sorption studies were also conducted for **MOR-2** with ReO_4^- solutions of low concentrations (~5.4 and 26.8 μM). The results indicated that **MOR-2** is capable of achieving ~78 and 91% ReO_4^- removal (in sorption studies with 5.4 and 26.8 μM initial ReO_4^- concentrations, respectively) and equilibrium is reached within 2–3 minutes (Fig. S4†).

The ReO_4^- sorption isotherms for **MOR-1** and **MOR-2** (pH ~ 7) are shown in Fig. 2. It can be clearly seen that the maximum sorption capacity for **MOR-2** is more than double that of **MOR-1**. Indeed, fitting of the isotherm data with the Langmuir–Freundlich equation (Fig. S5 and S6†) revealed maximum ReO_4^- sorption capacities of 4.10 ± 0.40 and 1.47 ± 0.07 mmol g^{-1} for **MOR-2** and **MOR-1**, respectively. The isotherm sorption data for **MOR-2** were also determined in acidic solutions (pH ~ 2) and the results revealed a high sorption efficiency of the material with the maximum ReO_4^- sorption capacity found to be 3.2 ± 0.2 mmol g^{-1} (Fig. S7†). To

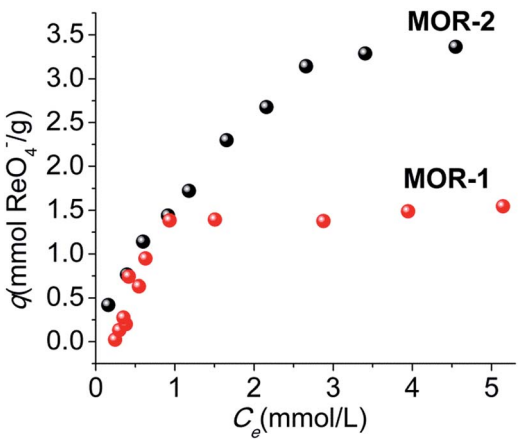

Fig. 2 Isotherm ReO_4^- sorption data (pH ~ 7) for MOR-1 and MOR-2 materials. C_e (mmol L^{-1}) represents the equilibrium ReO_4^- concentration of the solutions (*i.e.* that determined after the sorption process).

simulate conditions existing in highly acidic nuclear waste,[21] ReO_4^- sorption investigations for **MOR-2** were also conducted in 1 M HNO_3 solutions. Remarkably, the maximum ReO_4^- sorption capacity found for **MOR-2** under such extremely acidic conditions was 3.6 ± 0.3 mmol g^{-1} (Fig. S8†), *i.e.* very similar to ReO_4^- sorption capacities determined in neutral aqueous media and solutions with pH ~ 2. The exceptional sorption capacity of **MOR-2** in highly acidic aqueous media, in combination with its stability under extremely acidic conditions,[15] points to potential applications of this material for remediation of acidic nuclear waste.[21] The ReO_4^- sorption capacity of **MOR-2** significantly exceeds those reported for other metal organic materials (Fig. 3) showing perrhenate sorption capacities in the range 0.64–3.14 mmol ReO_4^- per g in neutral aqueous media.[9–13] Note that so far only one MOF (a Ag^+ compound) has shown ReO_4^- sorption capacity (~0.8 mmol g^{-1}) in acidic solutions (pH ~ 2),[10] which however is far less than that of **MOR-2** (3.2 ± 0.2 mmol g^{-1}) under similar conditions (Fig. 3). In addition, prior to our work no MOF has shown to be capable of capturing ReO_4^- in extremely acidic (pH ≤ 0) aqueous media (Fig. 3). Furthermore, **MOR-2** can be regenerated by treating the ReO_4^- loaded material with HCl solution and reused for ReO_4^- sorption, as will be discussed in the section for the column sorption data.

The ReO_4^- sorption capacity of **MOR-1** and **MOR-2** in the presence of competitive anions, such as Cl^-, Br^-, NO_3^- and SO_4^{2-}, was also determined. The monovalent anions (Cl^-, Br^-, and NO_3^-) have essentially no influence on the ReO_4^- sorption properties of the MOFs. Thus, the removal capacities found for **MOR-1** and **MOR-2** were ~50 and 70%, respectively (*i.e.* similar to those found in the absence of competitive anions), in the presence of a 10-fold excess of Cl^-, Br or NO_3^- (initial ReO_4 concentration ~ 0.58 mM) (Fig. S9†). Furthermore, **MOR-2** has shown excellent capability to absorb ReO_4^- even in the presence of a tremendous excess (130 to 600-fold excess) of NO_3^-, as revealed by the ReO_4^- isotherm sorption data in 1 M HNO_3 acid solutions (see above). This excellent selectivity of **MOR-2** for ReO_4^- *vs.* NO_3^- is attractive for remediation of nuclear waste often containing large quantities of nitrate anions.[10] The ReO_4^- sorption capability of **MOR-1** and **MOR-2** was not influenced in the presence of equimolar concentrations of SO_4^{2-} (ReO_4^- removal efficiencies were found to be 50 and 70% for **MOR-1** and **2**, respectively) (Fig. S9†). However, **MOR-1** and **MOR-2** showed 20.9 and 16.3% ReO_4^- removal capacities, respectively, in the presence of 5-fold excess of SO_4^{2-} (Fig. S9†). Sulphate, as a divalent anion and with capability to interact strongly with ammonium/pyridinium groups, seems to be a serious competitor for ReO_4^- sorption by **MOR-1** and **MOR-2**.

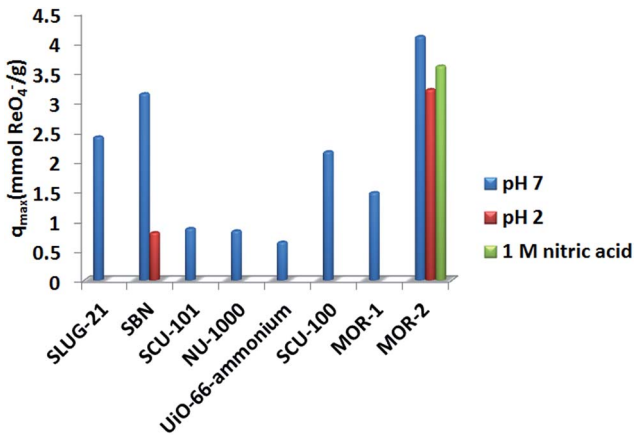

Fig. 3 Comparison of the ReO_4^- sorption capacities of MOR-1 and MOR-2 with those of reported metal organic materials.[9–13]

b. ReO_4^- column sorption studies

As a final step of the ReO_4^- sorption investigations, we have also studied the column ReO_4^- sorption properties, which are more relevant to practical applications. Note that the detailed column ReO_4^- sorption investigations for MOFs have not been conducted prior to our work.[9–13] Taking into account that batch sorption data revealed much higher sorption capacity for **MOR-2** than that of **MOR-1**, only **MOR-2** was tested for column sorption. However, as reported previously, **MOR-2** and other porous metal organic materials in their pristine form, with a few exceptions (*e.g.* a recently reported anion exchange MOF isolated as large single crystals[11a]), are not suitable to be used as stationary phases in ion exchange columns, as they have a strong tendency to form fine suspensions in water resulting in column clogging or/and loss of the active material.[18,19]

Thus, the column sorption investigations were performed on the composite of the **MOR-2** material with alginic acid (HA) which has improved mechanical properties that allow it to remain fixed in the column.[19] The stationary phase of the column tested for ReO_4^- consisted of a mixture of silica sand (~99% wt) and the **MOR-2–HA** composite (~1% wt) (Fig. 4, inset). Such an ion exchange column has been tested in our previous work for Cr(VI) sorption showing very promising results.[18,19] The column ReO_4^- sorption tests were performed with a solution of ReO_4^- with an initial concentration of 1.14 mM (pH ~ 7). ICP-MS data revealed that 10.5 mL of this solution passed through the column contained Re in concentrations ≤0.024 ppm (1.29 × 10^{-4} mM), which indicates the essential quantitative removal of ReO_4^- from the solution. The column can be regenerated by washing with 4 M HCl solution and then it can be reused showing almost identical sorption capacity with that found in the first run of the column. Remarkably, the column retains its initial sorption capability even after the fourth cycle of regeneration/reuse (Fig. 4). Thus, the breakthrough capacity,[18,19] was found identical (0.24 mmol g^{-1}, see ESI†) for all 4 runs of the column. The sorption data for the four successive column runs can be fitted with the Thomas model (Fig. S10, Table S1†)[18,19] and the results of the fitting revealed total column sorption capacities in the range from 0.33 to 0.37 mmol ReO_4^- per g.

c. TcO_4^- sorption studies

The above results indicated the high efficiency of **MOR-1** and (especially) **MOR-2** for ReO_4^- sorption and motivated us to continue our studies towards the investigation of these materials as TcO_4^- sorbents. Sorption experiments using ReO_4^-

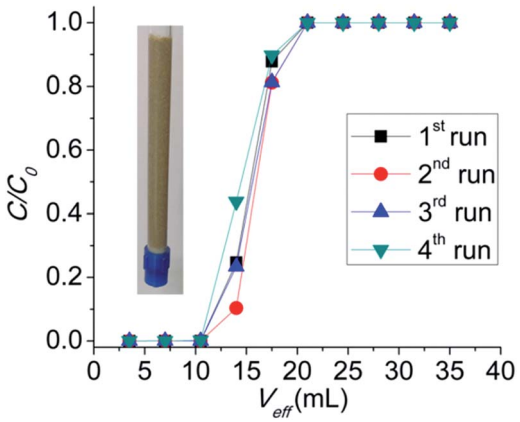

Fig. 4 Breakthrough curves for four column ion exchange runs (C = ReO_4^- concentration of the effluent, C_0 = initial ReO_4^- concentration = 1.14 mM, pH ~ 7, flow rate ~ 1.75 mL min^{-1}, one bed volume = 3.5 mL, and stationary phase **MOR-2**–**HA**/sand = 0.05 g:5 g). The lines are only a guide for the eye. Inset: photo of the ion exchange column used in the ReO_4^- sorption experiments.

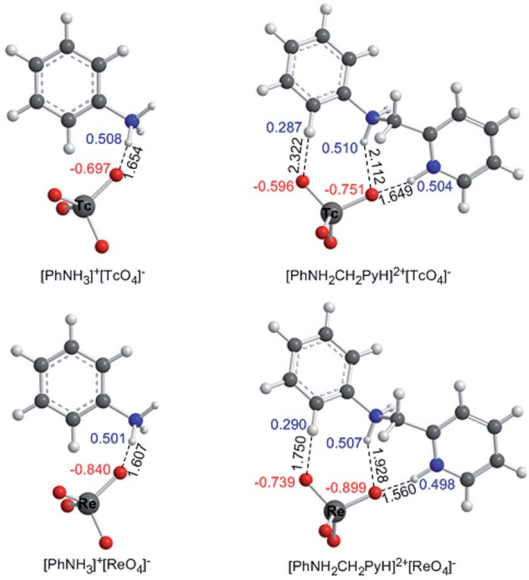

Fig. 5 Optimized geometries of the adducts formed between TcO_4^- and ReO_4^- with the $[PhNH_3]^+$ and $[PhNH_2CH_2PyH]^{2+}$ ligands (distances in Å, numbers in blue and red are positive and negative natural charges).

solutions with $^{99m}TcO_4^-$ as the tracer (see ESI†) were performed and the effect of the contact time was investigated at pH 2 in the time region 2–60 min. As it is shown in Fig. S11,† the sorption was very fast and the equilibrium was reached in 10 min for both **MOR-1** and **MOR-2**. The sorption isotherm data (Fig. S12†) for **MOR-1** and **MOR-2** (pH 2, dosage 15 mg of sorbent in 10 mL solution) revealed maximum sorption capacities of ~1.6 and 3.5 mmol g^{-1}, respectively, which are very close to the corresponding ReO_4^- sorption capacities of the MOFs reported above thus indicating ReO_4^- as an excellent non-radioactive surrogate for TcO_4^-. In addition, the effect of the background electrolyte was studied and it was observed that the presence of SO_4^{2-} (0.01 M Na_2SO_4) leads to a significant decrease in the uptake (about 80%), as also observed for the ReO_4^- sorption results described above. Regeneration of the sorbents was carried out using 4 M HCl, followed by washing with bi-distilled water. Then the materials were re-loaded in the second cycle and exhibited the same sorption capacity as in the first cycle.

d. Mechanism of ReO_4^-/TcO_4^- sorption

In order to elucidate the mechanism of ReO_4^-/TcO_4^- sorption by **MOR-1** and **MOR-2** combined, theoretical and experimental investigations were carried out.

i. Theoretical studies. The presence of chelating pyridylmethyl-ammonium functional groups of **MOR-2** could be one of the driving forces for the enhanced ReO_4^-/TcO_4^- sorption capability of this MOF. To this end, we performed DFT calculations using $[PhNH_3]^+$ and $[PhNH_2CH_2PyH]^{2+}$ substrates as models of the NH_3^+-BDC and H_2PATP ligands of **MOR-1** and **MOR-2**, respectively. The equilibrium geometries of 1 : 1 adducts formed upon interaction of the TcO_4^- and ReO_4^- anions with the model substrates, calculated at the wB97xd/ADZP(M)U6-31G+(d)(E) level of theory, are depicted schematically in Fig. 5 (details of the DFT calculations are given in the ESI†). Inspection of Fig. 5 reveals the formation of N–H···O hydrogen bridges between one amine proton of the $[PhNH_3]^+$ species and an O atom of the oxometalate anionic species. The binding energies of the interaction between TcO_4^- and ReO_4^- and the $[PhNH_3]^+$ substrate are estimated to be 13.2 and 17.6 kcal mol^{-1}, respectively, at the wB97xd/ADZP(M)U6-31G+(d)(E) level. Notice also that, calculations at the same level of theory revealed that NO_3^- and SO_4^{2-} anions interact with the $[PhNH_3]^+$ substrate with interaction energies equal to 15.1 and 23.5 kcal mol^{-1}, respectively. The higher interaction energy calculated for the SO_4^{2-} anion could be attributed to the fact that the latter forms two N–H···O hydrogen bridges with the $[PhNH_3]^+$ species in contrast to the NO_3^- anion which forms only one N–H···O hydrogen bridge, following the same structural bonding pattern as the TcO_4^- and ReO_4^- anions (Fig. S13 and S15†). On the other hand, in the 1 : 1 adducts $[PhNH_2CH_2PyH]^{2+}[MO_4]^-$ (M = Tc, Re), three hydrogen bridges, namely two N–H···O and one C–H···O are formed upon association of the $[PhNH_2CH_2PyH]^{2+}$ substrate with the oxometalate anionic species (Fig. 5). The estimated interaction energies for the $[PhNH_2CH_2PyH]^{2+}[MO_4]^-$ (M = Tc, Re) adducts are 23.0 and 26.4 kcal mol^{-1}, respectively, at the wB97xd/ADZP(M)U6-31G+(d)(E) level.

It is worth noting that the pertechnetate and perrhenate anions interact more strongly with $[PhNH_2CH_2PyH]^{2+}$ than with the $[PhNH_3]^+$ substrate due to the formation of three instead of one hydrogen bridges. The estimated interaction energies illustrate the stronger binding of ReO_4^- than that of TcO_4^- either to $[PhNH_2CH_2PyH]^{2+}$ or $[PhNH_3]^+$ substrates. This is also reflected on the calculated H···O distances of the hydrogen bridges which are shorter in the case of ReO_4^-. In addition, DFT calculations at the same level of theory, reveal that the NO_3^- and SO_4^{2-} anions interact with the $[PhNH_2CH_2PyH]^{2+}$ substrate with interaction energies equal to 23.4 and 38.6 kcal mol^{-1}, respectively. Remarkably, both SO_4^{2-} and NO_3^- anions form

two N–H···O hydrogen bridges with one of their O atoms (Fig. S13†).

In order to get a deeper insight into the nature of the intermolecular interactions between the ReO_4^- and TcO_4^- anions and the $[PhNH_3]^+$ and $[PhNH_2CH_2PyH]^{2+}$ substrates we employed natural bond orbital analysis (NBO), atoms in molecules (AIM) and reduced density gradient (RDG) calculations. The NBO analysis reveals the partial electrostatic character of the $MO_4^-\cdots[PhNH_3]^+$ and $MO_4^-\cdots[PhNH_2CH_2PyH]^{2+}$ (M = Tc or Re) associations due to the negative natural atomic charge on the O atoms of the anions and the positive natural atomic charge on the protons participating in the formation of the hydrogen bridges (Fig. 5). The O···H bonding interactions between the O atoms of the anions and the protons of the substrates is further confirmed by AIM analysis revealing existence of one bond critical point (BCP) located between each of them (BCPs A, B and C, Fig. S14†). In Table S2† are given the values of selected AIM parameters calculated for these BCPs. The magnitude of AIM BCP parameters points out (see Computational details in the ESI†) a closed shell type interaction, being an intermediate between ionic bond, hydrogen bond or van der Waals interaction. Finally, the RDG method specifies the presence of dispersion force interactions between O atoms of the anions and the protons of the substrates (Fig. S14†).

ii. Experimental studies. PXRD data (Fig. S15 and S16†) revealed that the ReO_4^--loaded materials (**MOR-1/ReO_4^-**, **MOR-2/ReO_4^-**) have almost identical structural features to pristine MOFs. The presence of perrhenate was clearly demonstrated *via* FT-IR spectroscopy indicating the existence of the characteristic strong ReO_4^- band at 912 and 914 cm^{-1} in the spectra of **MOR-1/ReO_4^-** and **MOR-2/ReO_4^-**, respectively (Fig. S17 and S18†).[22] EDS analytical data for **MOR-1/ReO_4^-** and **MOR-2/ReO_4^-** further confirmed the presence of Re in these materials (Fig. S19†).

Furthermore, the Brunauer–Emmett–Teller (BET) surface areas were determined for the ReO_4^--loaded materials and compared to those of pristine MOFs. Thus, the BET surface area for **MOR-1/ReO_4^-** was found to be 782 $m^2\ g^{-1}$ (Fig. S20†), which is ~29% decreased compared to that of the pristine MOF (1097 $m^2\ g^{-1}$). This indicates inclusion of ReO_4^- inside the pores of the MOF. A relatively moderate drop of the BET surface area of **MOR-1** after ReO_4^- sorption, in comparison with *e.g.* the substantial decrease (~96%) of the BET surface area of **MOR-1–HA** upon sorption of dichromate anions,[18] is probably due to the partial replacement of guest Cl^- anions by ReO_4^- species. Indeed, according to isotherm ReO_4^- sorption data ~4 ReO_4^- anions are inserted per formula unit of **MOR-1** (calculated capacity for sorption of $4ReO_4^-$ per $Zr_6O_4(OH)_4(NH_3^+\text{-BDC})_6Cl_6\cdot 35H_2O$ = 1.54 mmol g^{-1}; found = 1.47 ± 0.07 mmol g^{-1}). Thus, $2Cl^-$ anions per formula unit of **MOR-1** should not be exchanged (*i.e.* remain as guest species in the pores of the MOF) thus satisfying charge balance requirements. The presence of Cl^- anions in **MOR-1/ReO_4^-** is confirmed by EDS analytical data (Fig. S19†). Based on the above discussion, the ReO_4^--exchange process for **MOR-1** can be described by the following equation:

$$[Zr_6O_4(OH)_4(NH_3^+\text{-BDC})_6]Cl_6 + 4ReO_4^- \rightarrow [Zr_6O_4(OH)_4(NH_3^+\text{-BDC})_6](ReO_4)_4Cl_2 + 4Cl^- \quad (1)$$

The structure of **MOR-1/ReO_4^-** was determined and refined by PXRD methods. After successfully indexing the PXRD pattern, we were able to locate the Zr_6O_8 core and the position of Re by direct methods. Specifically, the Re species were found above the triangular face of the Zr_6O_8 octahedron at close proximity to the μ_3-O atom. Then, based on the direct methods solution we built a structural model, which was optimized and used as the starting point for the Rietveld refinement (details in the ESI†). The refinement results were very satisfying indicating the appropriateness of the proposed structural model (Fig. S21†). A part of the refined structure of **MOR-1/ReO_4^-** indicating the positions of ReO_4^- and Cl^- (not exchanged by ReO_4^-) anions is represented in Fig. 6.

The BET surface area for **MOR-2/ReO_4^-** was determined to be 280 $m^2\ g^{-1}$ (Fig. S22†), which is moderately (~21%) decreased compared to that of pristine **MOR-2** (354 $m^2\ g^{-1}$). Such a moderate drop of the BET surface area, determined after sorption of ReO_4^- species, has been also observed for NU-1000, which also possesses an eight-connected network.[12] Based on single crystal X-ray data, it was demonstrated that ReO_4^- anions are coordinated (mainly in a monodentate fashion) with the Zr_6 clusters of the Re(VII)-loaded NU-1000.[12] Therefore, **MOR-2**, exhibiting an eight-connected framework and easily exchangeable terminal OH^-/H_2O ligands,[19] may also be capable of binding Re(VII) species into the Zr_6 units. Note that the observed sorption capacity of 4.1 ± 0.4 mmol g^{-1} is relatively close to the value calculated for sorption of eight ReO_4^- anions per formula unit of **MOR-2** (~3.4 mmol g^{-1} for the complete exchange of eight Cl^- anions by ReO_4^- anions). Based on these results and literature data on eight-connected Zr^{4+} MOFs,[12,19] we propose that the absorbed ReO_4^- anions exchange not only the guest Cl^- species but also the eight terminal ligands in the Zr_6 clusters. This is described by the following equation:

$$H_{16}[Zr_6O_{16}(H_2PATP)_4]Cl_8 + 8ReO_4^- \rightarrow [Zr_6O_8(ReO_4)_8(H_2PATP)_4] + 8Cl^- + 8H_2O \quad (2)$$

An optimized structural model involving 8 monodentate ReO_4^- anions per Zr_6 unit was used as the starting point for the

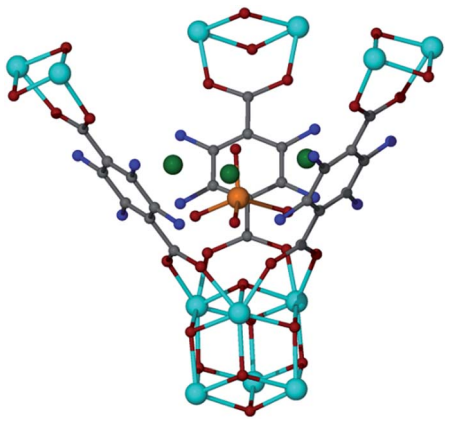

Fig. 6 The location of the perrhenate and chloride anions in the pyramidal pocket formed in **MOR-1/ReO_4^-**. Color code: Zr, sky blue; O, red; C, grey; N, blue; Re, orange; Cl, green.

Rietveld refinement and the results of the refinement were satisfactory (Fig. S23†) confirming the correctness of the proposed structural model (details of the crystal structure solution and refinement are given in the ESI†). A representation of the refined structure of **MOR-2/ReO_4^-** showing the coordination of 8ReO_4^- anions with the Zr_6 unit is given in Fig. 7.

It is obvious that ReO_4^- sorption mechanisms discussed above are expected to be valid also for TcO_4^- capture by **MOR-1** and **MOR-2** considering the close similarity between ReO_4^- and TcO_4^- sorption data found for these materials.

Overall, the experimental and theoretical results revealed that the excellent sorption capability of **MOR-2** is due to (a) its chelating functional groups with capability to interact strongly with ReO_4^-/TcO_4^- species facilitating the insertion of these species into the MOF's pores and (b) the presence of labile and easily exchangeable terminal OH^-/H_2O ligands in Zr_6 cluster units acting as intra-framework sorption sites for ReO_4^-/TcO_4^- anions.

iii. Explanation of selectivity of MOFs for ReO_4^-/TcO_4^-. From the theoretical studies, it is clear that the interactions of the MOFs' functional groups with the SO_4^{2-} anions are particularly strong. This is in accordance with the experimental sorption results revealing SO_4^{2-} as a strong competitor for the capture of ReO_4^-/TcO_4^- species by **MOR-1** and **MOR-2**. Not much difference, however, is observed between the interaction energy of ReO_4^- (or TcO_4^-) and that of NO_3^- with the functional groups of the MOFs. Therefore the high selectivity of the MOFs, especially **MOR-2**, for ReO_4^-/TcO_4^- *vs.* NO_3^- cannot be explained on the basis of their interactions with organic linkers. It is likely that ReO_4^-/TcO_4^- can bind more strongly than NO_3^- to the Zr_6 clusters in **MOR-2**, thus leading to the observed high selectivity for Re(VII)/Tc(VII) species. Indeed, the estimation of partial charges of atoms for ReO_4^-, TcO_4^- and NO_3^- *via* NBO analysis revealed a significantly higher negative charge on the O atoms of ReO_4^- and TcO_4^- (−0.773 and −0.630, respectively) *vs.* that of the corresponding atoms for NO_3^- (−0.572) (Fig. S24†). Thus, the O atoms of ReO_4^-, TcO_4^- are expected to interact more strongly with the hard Zr^{4+} ions and display more efficient ligation capability than NO_3^-. In comparison, the charge of sulphate oxygen atoms (−1.149) is higher than that of the corresponding atoms for ReO_4^-/TcO_4^- (Fig. S24†) and thus, SO_4^{2-} is expected to have the highest affinity for the Zr_6 clusters of **MOR-2**. This provides an additional explanation for the observed decreased sorption capability of **MOR-2** for ReO_4^-/TcO_4^- in the presence of excess of SO_4^{2-} anions.

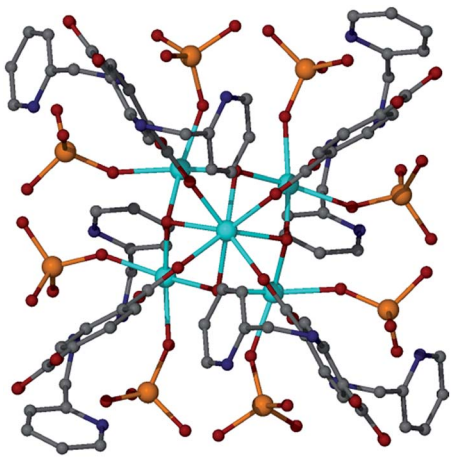

Fig. 7 Representation of the Zr_6 unit in **MOR-2/ReO_4^-** highlighting the presence of eight monodentate ReO_4^- ligands. Color code: Zr, sky blue; O, red; C, grey; N, blue; Re, orange; Cl, green.

e. ReO_4^- luminescence sensing

As mentioned above, the development of accurate, fast and sensitive sensors for the detection of ReO_4^- is important for the development and study of materials which can act as sorbents for ReO_4^-, the latter being a good surrogate for the radioactive pertechnetate anion. Thus, following the encouraging results from our previous work on the study of the protonated version of **MOR-2** as a fluorescent sensor for Cr(VI) anions,[19] we decided to investigate the fluorescence properties of **MOR-1** and **MOR-2** in the presence of ReO_4^-. Both materials exhibit emission quenching in the presence of ReO_4^- with **MOR-2** showing markedly better response towards both in terms of higher sensitivity and reduced interference from competing anions. We therefore begin our discussion with the sensing properties of **MOR-2**.

In Fig. 8 we see the result of the fluorescence titration of an aqueous suspension of **MOR-2** (~0.1 mg mL^{-1}), previously activated by treatment with 4 N HCl (see ESI† for details), with ReO_4^- anions. The initial ligand-based[23] fluorescence signal of **MOR-2** (λ_{em} = 460 nm) is strongly quenched upon the addition of increasing concentrations of ReO_4^- anions with a concomitant slight blue shift of the emission maximum by about 5 nm. By measuring the integrated fluorescence intensities before and after exposure to ReO_4^-, I_0 and I, respectively, we determined

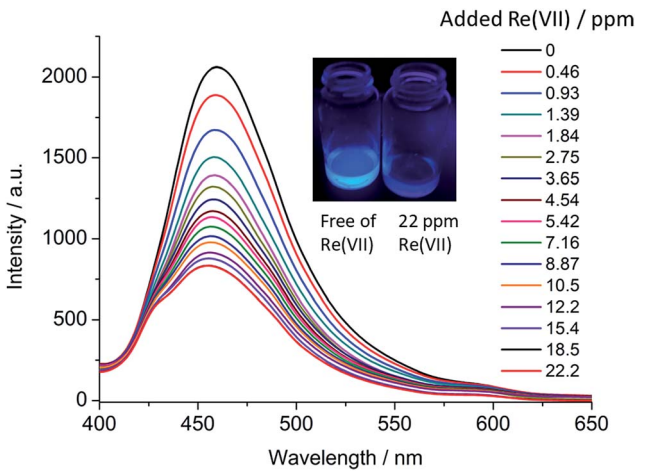

Fig. 8 Fluorescence titration (λ_{exc} = 360 nm) of activated **MOR-2** suspended in water upon the gradual addition of a 10^{-3} M aqueous solution of NH_4ReO_4. The experiment was carried out at pH 5. The numbers correspond to the total added Re(VII) in ppm. The inset shows a photograph of two samples of **MOR-2** suspended in water at pH 5 (0.1 mg mL^{-1}) and illuminated with a standard laboratory UV lamp (360 nm). The sample in the left is free of Re(VII) while the one in the right contains 22 ppm Re(VII).

a quenching percentage, $(I_0 - I/I_0) \times 100$, of 63% at the end of the titration [*ca.* 22 ppm of Re(VII)].

The calibration curve of the fluorescence titration (Fig. S25†) shows a good linearity ($R^2 > 0.99$) in the 0–2 ppm concentration range and its slope corresponds to the limits of detection (LOD) and quantification (LOQ) of 0.15 and 0.51 ppm, respectively. The LOD values are markedly lower than those obtained in UV-vis spectrophotometric methods of ReO_4^- determination (3–4 ppm).[24] Furthermore, the fluorimetric detection of ReO_4^- presents the additional advantage of the lack of need for time consuming sample pre-treatment often required in colorimetric methods (*vide supra*) thereby allowing real-time detection of ReO_4^-.

To determine whether the presence of other anions has a deleterious effect on the ability of **MOR-2** to function as a fluorescent sensor for ReO_4^-, we performed titration experiments where aqueous suspensions of **MOR-2** were titrated with a 10^{-3} M solution of ReO_4^- [corresponding to 186 ppm Re(VII)] containing an excess of Cl^- (10^{-2} M), NO_3^- (10^{-2} M) and SO_4^{2-} (2×10^{-3} M) anions, which are commonly present in real water samples. In agreement with the sorption results (*vide supra*), Cl^- and NO_3^- had virtually no effect (Fig. S26 and S27†) on the sensing ability of **MOR-2** towards ReO_4^- in both detection limit and maximum quenching percentage (0.17 ppm and 60%, respectively). Remarkably, when the analyte solution contained a 2-fold excess of SO_4^{2-} ions (Fig. S28†), we observed only a slight increase in LOD and LOQ values of **MOR-2** (0.20 and 0.65 ppm, respectively) even though, as demonstrated in the sorption studies, sulfates substantially decrease the ability of **MOR-2** to interact with ReO_4^- ions. An explanation for this observation may be provided by considering the fact that even though **MOR-2** sorbs both SO_4^{2-} and ReO_4^- anions, only the latter is able to efficiently quench the material's fluorescence. Therefore, even though competition with SO_4^{2-} leads to the interaction of a smaller portion of the material's chromophores with ReO_4^-, a similarly strong detection signal is obtained as exciton migration leads to signal amplification (*vide supra*).

To further assess the sensing ability of **MOR-2** towards Re(VII) in real samples, we performed an additional sensing experiment using potable water containing 4.0 ppm of the main competing anion SO_4^{2-} as both the solvent for the 10^{-3} M ReO_4^- stock solution and the suspension medium for **MOR-2**. As seen in Fig. S29† the use of potable water similarly has only a limited effect on the performance of **MOR-2** as a sensor for ReO_4^- ions (LOD and LOQ are 0.19 and 0.64 ppm, respectively).

Identical sensing experiments performed on **MOR-1** (Fig. S30–S34†) revealed that the latter material also displays a response towards ReO_4^-. As seen in Fig. 9, the fluorescence titration of **MOR-1** results in the strong quenching of the material's emission (62% quenching at the end of the titration). The calibration curve shows excellent linearity in the 0–3 ppm concentration range, albeit with about half the gradient of that of **MOR-2** (Fig. S30†). Consequently, the LOD and LOQ values for **MOR-1** are 0.36 and 1.2 ppm, respectively, still noticeably lower than the values typically obtained in colorimetric methods (*vide supra*). As in the case of **MOR-2**, Cl^- and NO_3^- ions do not have a significant effect on the ability of **MOR-1** to

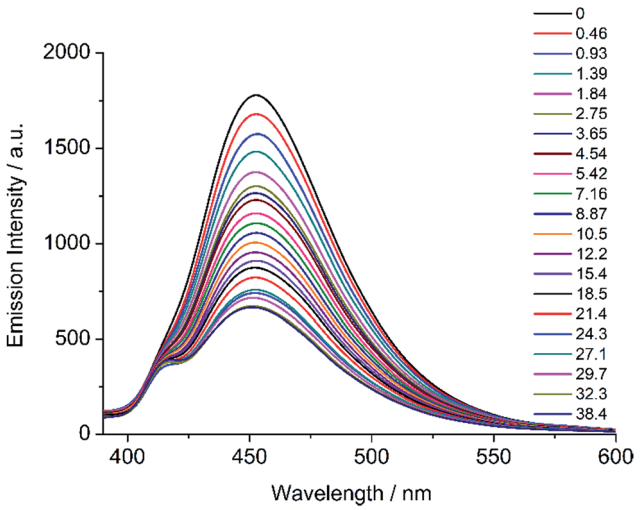

Fig. 9 Fluorescence titration (λ_{exc} = 360 nm) of activated **MOR-1** suspended in water upon the gradual addition of a 10^{-3} M aqueous solution of NH_4ReO_4. The experiment was carried out at pH 5. The numbers correspond to the total added Re(VII) in ppm.

detect ReO_4^- (Fig. S31 and S32†). In potable water (Fig. S34†), where 4 ppm of SO_4^- is present throughout the titration, we observe only a slight increase in the LOD value (0.46 ppm). However, it should be noted that the saturation point of the titration is reached at a much lower concentration of ReO_4^- in comparison to the experiments conducted in pure water (*ca.* 12 ppm *versus ca.* 38 ppm) and the overall quenching percentage is also substantially lower (35%). This observation may be attributed to the partial occupation of the sorption sites of **MOR-1** by the competing SO_4^{2-} ions. The generally decreased sensing performance of **MOR-1** in comparison to that of **MOR-2** is in good agreement with the sorption studies which showed that the latter material is a better sorbent for ReO_4^-.

Additionally, in the light of our structural studies (*vide supra*) showing that ReO_4^- binds as a terminal ligand to the open coordination sites of the eight-connected $Zr(IV)_6$ clusters of **MOR-2**, we may conclude that the incorporation of Re(VII) renders the $Zr(IV)_6$ clusters better electron acceptors thereby increasing the efficiency of ligand-to-cluster electron transfer which leads to fluorescence quenching.[23]

In order to provide further confirmation that the observed emission quenching in **MOR-1** and **MOR-2** is indeed due to the interaction of their chromophores with ReO_4^-, we performed control experiments where the active ion exchange groups of both materials were deprotonated by treatment with excess triethylamine in methanol thereby rendering them incapable of interacting with anions. As shown in Fig. S35,† the emission spectra of the deactivated materials are virtually not affected by the presence of up to 37 ppm Re(VII). These experiments emphasize the importance of the initial ion exchange step which is essential in order to bring the analyte within the material's cavities.

Furthermore, inspection of the UV-Vis absorption spectrum of ReO_4^- (Fig. S36†) reveals that it is devoid of any features at wavelengths above *ca.* 280 nm and thus does not overlap with

the emission spectra of **MOR-1** and **MOR-2** or the excitation wavelength of 360 nm employed in our fluorescence studies. This precludes quenching by either radiationless or radiative bridging ligand-to-ReO_4^- energy transfer.[16] Even though ReO_4^- ions are much weaker oxidants than the oxoanions of lighter metals such as Mn(VII) and Cr(VI), they have shown to quench the fluorescence of the molybdate binding ModA protein possibly *via* tyrosine-to-ReO_4^- electron transfer.[25] We therefore conclude that bridging ligand-to-ReO_4^- electron transfer is most possibly responsible for the observed fluorescence quenching. At this point we should also note that **MOR-2** shows a higher sensing ability by more than an order of magnitude towards Cr(VI) oxoanions[19] compared to ReO_4^- most probably reflecting the far greater oxidizing ability of the former. This precludes efficient detection and determination of ReO_4^- in the presence of significant concentrations of Cr(VI) species. However, this limitation can potentially be tackled by suitable sample pretreatment which would selectively remove Cr(VI) anions without affecting the concentration of Re(VII). One such method would be the precipitation of chromate anions in the form of the insoluble $Ba(CrO_4)$ by treatment of the sample with $Ba(NO_3)_2$. The significant solubility of $Ba(ReO_4)_2$ would ensure that ReO_4^- ions remain in the solution.[26]

Conclusions

In conclusion, a detailed investigation of ReO_4^-/TcO_4^- sorption properties of two Zr^{4+} MOFs **MOR-1** and **MOR-2** was performed. Despite **MOR-2** being significantly less porous compared to **MOR-1**, it shows much more efficient ReO_4^-/TcO_4^- exchange properties. Particularly, **MOR-2** displays the highest ReO_4^-/TcO_4^- sorption capacities reported among MOFs and more importantly, it shows excellent capability for removal of these anions under extremely acidic conditions often found in nuclear waste. This is a result of multiple and strong hydrogen-bonding interactions of ReO_4^-/TcO_4^- anions with the functional groups of **MOR-2** and the presence of labile terminal ligands in the Zr_6 clusters that can be exchanged by ReO_4^-/TcO_4^- anions.

In addition to their sorption properties, **MOR-1** and **MOR-2** exhibit fluorescence quenching upon their interaction with ReO_4^- ions most possibly due to bridging ligand-to-ReO_4^- electron transfer. Fluorescence titration experiments showed that **MOR-2** shows the most promising properties as a fluorescent sensor for Re(VII) achieving limits of detection and quantification of 0.20 and 0.65 ppm, respectively, in the presence of moderate concentrations of competitive SO_4^{2-} ions. Actually, in this work for the first time we introduce MOFs as luminescent sensors for real-time, selective detection/determination of traces of ReO_4^- in aqueous media.

Overall, the results of the present studies indicate that the development of MOFs with highly efficient ReO_4^-/TcO_4^- ion sorption capacity and luminescence sensing capability for ReO_4^- should rely on the synergistic effects of functional groups with a high affinity for the targeted ions and intra-framework ion sorption sites. Efforts to develop new selective MOF sorbents/sensors for toxic ions and radionuclides are made continuously by our group.

Conflicts of interest

There are no conflicts to declare.

Acknowledgements

The powder X-ray diffraction and thermal analysis units of the Network of Research Supporting Laboratories at the University of Ioannina are acknowledged. The post-doctoral research of Dr A. Pournara was implemented with IKY scholarship, funded by the Act "Supporting Post-Academic Researchers" from the resources of the NF "Human Resources Development, Education and Lifelong Learning" with Priority Axes 6, 8, 9 and co-funded by the European Social Fund – ESF and the Greek State. Metal analysis performed at the Northwestern University Quantitative Bio-element Imaging Center was generously supported by the NASA Ames Research Center Grant NNA04CC36G. MGK would like to acknowledge the grant NSF DMR-1708254.

Notes and references

1 J. H. Lehr, M. Hyman, T. E. Gass and W. J. Seevers, *Handbook of complex environmental remediation problems*, McGraw-Hill New York, 2002.
2 D. Banerjee, D. Kim, M. J. Schweiger, A. A. Kruger and P. K. Thallapally, *Chem. Soc. Rev.*, 2016, **45**, 2724.
3 B. J. Riley, J. Chun, W. Um, W. C. Lepry, J. Matyas, M. J. Olszta, X. Li, K. Polychronopoulou and M. G. Kanatzidis, *Environ. Sci. Technol.*, 2013, **47**, 7540.
4 D. Banerjee, S. K. Elsaidi, B. Aguila, B. Li, D. Kim, M. J. Schweiger, A. A. Kruger, C. J. Doonan, S. Ma and P. K. Thallapally, *Chem.–Eur. J.*, 2016, **22**, 17581.
5 J. J. Neeway, R. M. Asmussen, A. R. Lawter, M. E. Bowden, W. W. Lukens, D. Sarma, B. J. Riley, M. G. Kanatzidis and N. P. Qafoku, *Chem. Mater.*, 2016, **28**, 3976.
6 (*a*) P. Kumar, A. Pournara, K.-H. Kim, V. Bansal, S. Rapti and M. J. Manos, *Prog. Mater. Sci.*, 2017, **86**, 25; (*b*) M. Mon, R. Bruno, J. Ferrando-Soria, D. Armentano and E. Pardo, *J. Mater. Chem. A*, 2018, **6**, 4912; (*c*) A. V. Desai, B. Manna, A. Karmakar, A. Sahu and S. K. Ghosh, *Angew. Chem.*, 2016, **128**, 7942; (*d*) Q. Gao, J. Xu and X.-H. Bu, *Coord. Chem. Rev.*, 2018, DOI: 10.1016/j.ccr.2018.03.015.
7 (*a*) S. Sarri, P. Misaelides, D. Zamboulis, X. Gaona, M. Altmaier and H. Geckeis, *J. Radioanal. Nucl. Chem.*, 2016, **307**, 681; (*b*) J. Li, X. Dai, L. Zhu, C. Xu, D. Zhang, M. A. Silver, P. Li, L. Chen, Y. Li, D. Zuo, H. Zhang, C. Xiao, J. Chen, J. Diwu, O. K. Farha, T. E. Albrecht-Schmitt, Z. Chai and S. Wang, *Nat. Commun.*, 2018, **9**, 3007; (*c*) P. Samanta, P. Chandra, S. Dutta, A. V. Desai and S. K. Ghosh, *Chem. Sci.*, 2018, DOI: 10.1039/c8sc02456a.
8 J. Li, X. Wang, G. Zhao, C. Chen, Z. Chai, A. Alsaedi, T. Hayat and X. Wang, *Chem. Soc. Rev.*, 2018, **47**, 2322.
9 H. Fei, M. R. Bresler and S. R. Oliver, *J. Am. Chem. Soc.*, 2011, **133**, 11110.
10 L. Zhu, C. Xiao, X. Dai, J. Li, D. Gui, D. Sheng, L. Chen, R. Zhou, Z. Chai, T. E. Albrecht-Schmitt and S. Wang, *Environ. Sci. Technol. Lett.*, 2017, **4**, 316.

11 (*a*) L. Zhu, D. Sheng, C. Xu, X. Dai, M. A. Silver, J. Li, P. Li, Y. Wang, Y. Wang, L. Chen, C. Xiao, J. Chen, R. Zhou, C. Zhang, O. K. Farha, Z. Chai, T. E. Albrecht-Schmitt and S. Wang, *J. Am. Chem. Soc.*, 2017, **139**, 14873; (*b*) D. Sheng, L. Zhu, C. Xu, C. Xiao, Y. Wang, Y. Wang, L. Chen, J. Diwu, J. Chen, Z. Chai, T. E. Albrecht-Schmitt and S. Wang, *Environ. Sci. Technol.*, 2017, **51**, 3471.

12 R. J. Drout, K. Otake, A. J. Howarth, T. Islamoglu, L. Zhu, C. Xiao, S. Wang and O. K. Farha, *Chem. Mater.*, 2018, **30**, 1277.

13 D. Banerjee, W. Xu, Z. Nie, L. E. Johnson, C. Coghlan, M. L. Sushko, D. Kim, M. J. Schweiger, A. A. Kruger and C. J. Doonan, *Inorg. Chem.*, 2016, **55**, 8241.

14 (*a*) D. Liu, K. Lu, C. Poon and W. Lin, *Inorg. Chem.*, 2014, **53**, 1916; (*b*) S. A. Diamantis, A. Margariti, A. D. Pournara, G. S. Papaefstathiou, M. J. Manos and T. Lazarides, *Inorg. Chem. Front.*, 2018, **5**, 1493; (*c*) W. P. Lustig, S. Mukherjee, N. D. Rudd, A. V. Desai, J. Li and S. K. Ghosh, *Chem. Soc. Rev.*, 2017, **46**, 3242.

15 S. W. Thomas, G. D. Joly and T. M. Swager, *Chem. Rev.*, 2007, **107**, 1339.

16 V. Balzani, P. Ceroni and A. Juris, *Photochemistry and photophysics: concepts, research, applications*, John Wiley & Sons, 2014.

17 (*a*) G. Dutta and B. Sur, *Microchim. Acta*, 1986, **88**, 359; (*b*) R. J. Thompson, R. H. Gore and F. Trusell, *Anal. Chim. Acta*, 1964, **31**, 590.

18 (*a*) S. Rapti, A. Pournara, D. Sarma, I. T. Papadas, G. S. Armatas, A. C. Tsipis, T. Lazarides, M. G. Kanatzidis and M. J. Manos, *Chem. Sci.*, 2016, **7**, 2427; (*b*) S. Rapti, A. Pournara, D. Sarma, I. T. Papadas, G. S. Armatas, Y. S. Hassan, M. H. Alkordi, M. G. Kanatzidis and M. J. Manos, *Inorg. Chem. Front.*, 2016, **3**, 635.

19 S. Rapti, D. Sarma, S. A. Diamantis, E. Skliri, G. S. Armatas, A. C. Tsipis, Y. S. Hassan, M. Alkordi, C. D. Malliakas, M. G. Kanatzidis, T. Lazarides, J. C. Plakatouras and M. J. Manos, *J. Mater. Chem. A*, 2017, **5**, 14707.

20 J. H. Cavka, S. Jakobsen, U. Olsbye, N. Guillou, C. Lamberti, S. Bordiga and K. P. Lillerud, *J. Am. Chem. Soc.*, 2008, **130**, 13850.

21 J. D. Law, R. S. Herbst and T. A. Todd, *Sep. Sci. Technol.*, 2002, **37**, 1353.

22 M. R. Mohammad and W. F. Sherman, *J. Phys. C: Solid State Phys.*, 1981, **14**, 283.

23 D. Sun, Y. Fu, W. Liu, L. Ye, D. Wang, L. Yang, X. Fu and Z. Li, *Chem.–Eur. J.*, 2013, **19**, 14279.

24 B. A. Lenell and Y. Arai, *Talanta*, 2016, **150**, 690.

25 B. P. Aryal, P. Brugarolas and C. He, *J. Biol. Inorg Chem.*, 2012, **17**, 97.

26 (*a*) L. Gordon and F. H. Firsching, *Anal. Chem.*, 1954, **26**, 759; (*b*) S. K. Majumdar, R. A. Pacer and C. L. Rulfs, *J. Inorg. Nucl. Chem.*, 1969, **31**, 33.